JOURNAL OF CATALYSIS **169,** 240–249 (1997)
ARTICLE NO. CA971634

Filamentous Carbon Formation and Gasification: Thermodynamics, Driving Force, Nucleation, and Steady-State Growth

J.-W. Snoeck,* G. F. Froment,†,[1] and M. Fowles‡

*BASF Antwerpen, Scheldelaan 600, B-2040 Antwerpen, Belgium; †Laboratorium voor Petrochemische Techniek, Universiteit Gent, Krijgslaan 281, B-9000 Gent, Belgium; and ‡ICI KATALCO, P.O. Box 1, Billingham, Cleveland, TS23 1LB, England

Received May 28, 1996; revised January 29, 1997; accepted February 3, 1997

A detailed description is given of the formation and the gasification of filamentous carbon. The diffusion of carbon through nickel originates from a concentration gradient, which implies a different solubility at the nickel–gas and the nickel–carbon interface. A thermodynamic basis for the different solubilities is provided. The segregation of carbon, taking place at the gas side of the nickel particle, is added as one of the steps in the global mechanism of carbon filament formation and gasification. The segregation process may be described in a way similar to that of gas adsorption. The coupling of the surface reactions, the segregation process, and the diffusion of carbon through the nickel particle leads to a detailed model of the process of carbon filament formation, which forms the basis for the kinetic modeling of carbon formation and gasification reactions. Experimental results for the methane cracking revealed that the number of carbon filaments that is able to nucleate strongly depends upon the affinity for carbon formation. © 1997 Academic Press

INTRODUCTION

Coke formation on catalysts and reactor tubes is an important problem in a variety of processes such as steam reforming and methanation, but also in the steam cracking of hydrocarbons (1–3). Coke formation may cause deactivation of the catalyst surface, blocking of catalyst pores and voids, or also physical desintegration of the catalyst support (2).

Various types of carbon may be formed. By temperature-programmed hydrogenation of carbon deposits on nickel catalysts, arising from ethylene and carbon monoxide, McCarty *et al.* (4, 5) distinguished up to seven different types of carbon. In steam reforming, the most important type of carbon is filamentous carbon (3). Its strength is such that it may destroy the catalyst support structure, leading to blockage of the reactor (2, 3). According to Boellaard *et al.* (8), the strength of filamentous carbon results from its conically ordered graphite layers.

Filamentous carbon has received considerable attention in the past 25 years. The most important topics of research were the thermodynamics of carbon filament formation (6, 9–12), the driving force for carbon diffusion (7, 12–19) and also the initiation of carbon filament growth and its detailed growth mechanism (6–8, 10, 12, 16–26).

The thermodynamic properties of filamentous carbon differ from those of graphite (6, 9–12). Rostrup-Nielsen (10) explained the deviation by the disordered structure of the filaments and the contribution of the surface energy of the high-area filaments, while Tibbetts (26) and Alstrup (12) also considered the elastic energy effect. De Bokx *et al.* (6) and Manning *et al.* (11) proposed that the observed deviation from the graphite equilibrium is due to the formation of an intermediate carbide phase. They explain the deviation from the graphite equilibrium by the formation of a phase, which is not the final product, with different thermodynamic properties.

The driving force for the bulk diffusion of carbon through the metal particle is ascribed either to a temperature gradient (18, 19) or to a concentration gradient (7, 12, 13, 16). Rostrup-Nielsen *et al.* (13) proposed that the carbon solubility at the gas/metal interface differs from that at the metal/carbon interface, since the activity of carbon in the gas phase may be much higher than one. Sacco *et al.* (16) suggest that the mass flux originates from the solubility difference between carbon at the α-iron/Fe_3C interface and that between α-iron and carbon itself. Kock *et al.* (7) propose that the driving force for bulk carbon diffusion is the gradient of the carbon content of sub-stoechiometric carbides, whereby the carbon content decreases in the direction of the metal/carbon interface. Central in the model of Alstrup (12) is the assumption, proposed by Schouten *et al.* (27), that the carbon atoms entering the selvedge create a "surface carbide."

In the present paper, a detailed description of the carbon filament formation is presented. The segregation equilibrium at the metal/gas interface is taken into account, while a thermodynamic basis for the difference in solubility at the metal/gas and the metal/carbon interface is proposed.

[1] To whom correspondence should be addressed.

0021-9517/97 $25.00

Methane cracking experiments on a supported nickel catalyst provided information on the nucleation of filamentous carbon, in particular on the influence of the coking conditions on the number of carbon filaments. This information was revealed by applying several carbon formation conditions sequentially on the same catalyst sample, followed by a gasification with hydrogen.

EXPERIMENTAL

Materials

The catalyst used in this study was the ICI KATALCO 46-9P steam reforming catalyst. This is a nickel catalyst promoted with low levels of potash to prevent carbon deposition during use. The catalyst is produced in the form of Raschig rings, which were broken into small pieces before use.

From N_2 adsorption at 77 K, a BET surface area of 13.7 m^2/g_{cat} was obtained. Mercury porosimetry led to a cumulative intruded pore volume of 0.1969 cm^3/g_{cat} and an average pore radius of 57.5 nm. The apparent density of the catalyst was 2042 kg/m_p^3, while a solid density of 3228 kg/m_s^3 was determined by He-pycnometry.

The gases with a purity >99.95% were purchased from L'Air Liquide.

Apparatus

The experiments were performed in an electrobalance unit, consisting of three main sections: the feed section, the reactor section, and the analysis section (Fig. 1). The reactor section comprised the preheater/vaporizer, the bypass valves, the reactor, the electrobalance, and the pressure regulation. The reactor was made out of stainless steel (i.d. 18.9 mm). Three infrared heaters, each controlled by a wall thermocouple, supplied the heat to maintain the reactor at the desired temperature. A catalyst-filled basket (diameter, 14.2 mm; mesh size, 0.225 mm) was suspended by nonmagnetic wires to one arm of the electrobalance (Sartorius Series 70). The diameter of the catalyst particles ranged from 0.25 to 0.50 mm. With this catalyst size, no diffusional limitations were encountered. A thermocouple was positioned just below the basket so as to measure the reaction temperature. An inert-filled basket in the reference chamber was suspended to the other arm of the electrobalance. The balance housing could be used up to 150 bar, and a sensitivity of 0.1 μg could be reached. A water cooling jacket kept the balance at room temperature. Valves enabled the reactant mixture to be directed either through the reactor or through the bypass. The flow rates of the gases were controlled by Brooks mass flow controllers. The gases flowed through the

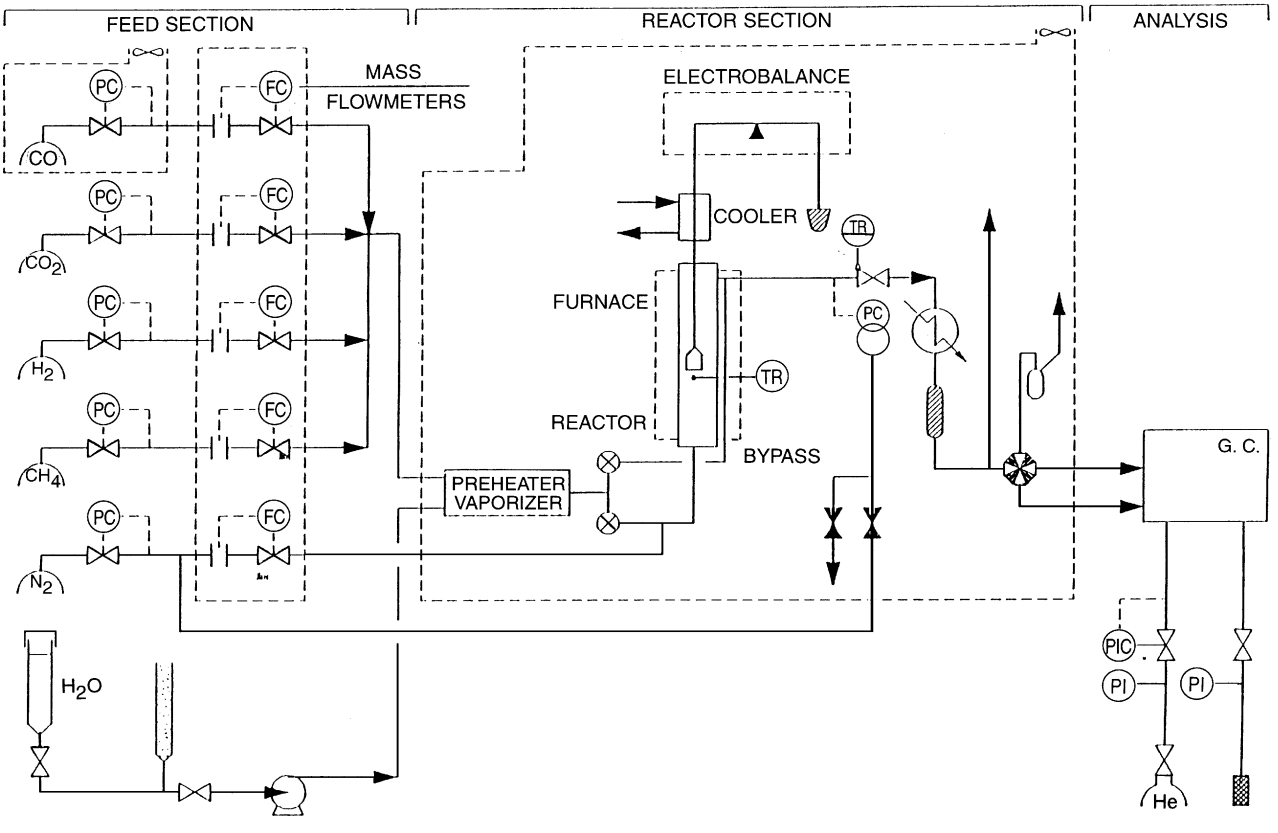

FIG. 1. Flow sheet of the experimental installation.

reactor from bottom to top. A blanketing gas prevented the hot gases from entering the balance chamber. The reactor effluent and the blanketing gas or the bypass effluent were led through one-way valves into the back pressure regulator. The effluent then flowed to the cooler/condensor, where water was condensed and collected. Water was present in the feed and the effluent when carbon formation experiments were performed with steam reforming mixtures. The dry effluent gas was then partly vented, while a small fraction was directed after drying to the gas chromatograph (Packard 439).

Experimental Procedure

The experimental procedure involved catalyst reduction, coking, and eventually also gasification. The catalyst was reduced in a 50 mol% H_2/N_2 mixture, while raising the temperature from ambient temperature to 700°C with a slope of 15°C/min, and maintaining the temperature for 45 min at 700°C.

The progress of the coking or the gasification were continuously monitored on the balance analog recorder, so that weight versus time curves were obtained. The rates of carbon formation or gasification were obtained from the slopes of the weight versus time curves. Since an important part of the feed bypasses the catalyst-filled basket, differential operation is required.

In the present work, filamentous carbon was formed by the cracking of methane and gasified by hydrogen.

RESULTS AND DISCUSSION

Mechanism of Carbon Filament Formation

The mechanism proposed in this work is schematically represented in Fig. 2. The surface reactions, such as the methane cracking or the Boudouard reaction, produce adsorbed carbon atoms. These isolated adsorbed carbon atoms were identified by McCarty *et al.* (4, 5) using

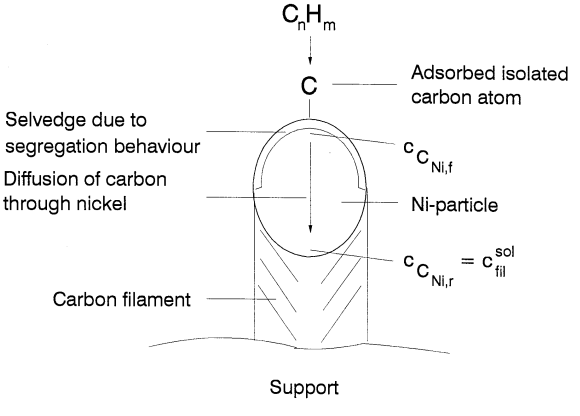

FIG. 2. Schematic representation of the mechanism of filamentous carbon formation.

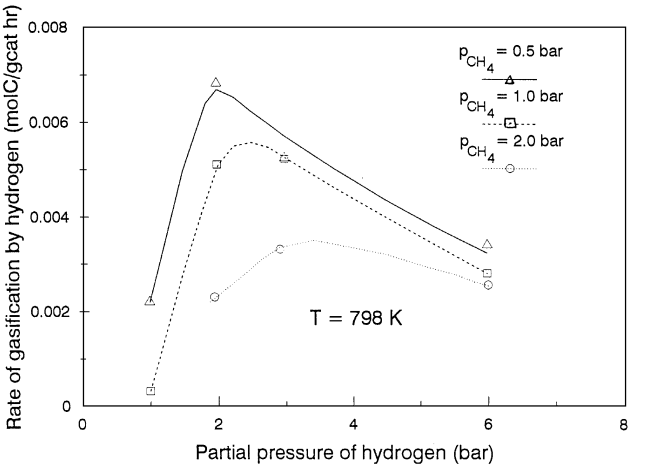

FIG. 3. Rate of gasification with hydrogen as a function of the partial pressure of hydrogen. Catalyst, ICI 46-9S; $T = 798$ K; $p_{CH_4} = 0.5$, 1, and 2 bar.

temperature-programmed hydrogenation (α and α' state). Other types of surface carbon which may encapsulate the surface can also be formed. The isolated surface carbon atoms which are important in the filament formation dissolve into the nickel particle at the gas side, and diffuse to the rear, at the support side. At the front of the nickel particle, a selvedge with high concentration is created because of the segregation behavior of carbon in nickel: the surface is enriched with carbon, and the carbon concentration decreases from the surface concentration to the bulk concentration of interstitially dissolved carbon over a number of atomic layers. The relation between the surface coverage of carbon and the bulk concentration of interstitially dissolved carbon in nickel, just below the selvedge, can be described by a segregation isotherm. Several types were presented by Laguës *et al.* (28). In the present work a Langmuir isotherm (in the case of segregation often named the Langmuir–McLean isotherm) is chosen on the basis of observations of Yang *et al.* (18), Isett *et al.* (29, 30), and Vajo *et al.* (31). Isett *et al.* and Vajo et al. proved that the segregation of carbon dissolved in nickel to the (100) surface can be described up to high coverages by the Langmuir isotherm, while Yang *et al.* showed by TEM/SAED that the (100) faces are the most abundant at the metal/gas interface during carbon filament formation on Ni. With this approach, carbon atoms, segregating from the solution to the surface, have to compete with gas phase atoms for the same surface sites. This is clearly illustrated by a selection of results for the gasification by hydrogen of filamentous carbon, deposited under standard conditions by the methane cracking, at different partial pressures of hydrogen (Fig. 3). The rate of gasification shows a maximum as a function of the partial pressure of hydrogen, due to the decrease of the surface coverage of carbon. If carbon would segregate from the bulk to separate sites, its coverage would not be influenced by the presence

of hydrogen. Alstrup (12) also assumed the existence of a selvedge with high concentration of carbon, which was called a "surface carbide."

The diffusion of carbon through the nickel particle is ascribed to the diffusion of interstitially dissolved carbon in nickel. The model with substoechiometric intermediate carbides, proposed by Kock *et al.* (7) seems unrealistic for nickel, since carbides are known to decompose above 350°C and could not be identified unambiguously during steady-state carbon filament formation. These intermediate carbides can certainly not be present when there is no affinity for carbon formation, namely during the gasification of filamentous carbon.

A carbon filament precipitates at the support side of the nickel particle. Boellaard *et al.* (18) showed that it is formed by the continuous excretion of carbon layers perpendicular to the metal/carbon interface and slipping of carbon layers.

Driving Force for Carbon Diffusion through Nickel

As mentioned in the Introduction, conflicting ideas exist concerning the driving force for carbon diffusion. Both Rostrup-Nielsen *et al.* (13) and Sacco *et al.* (16) proposed that the driving force is the difference in solubility of carbon at the gas/metal and the metal/filament interface. A thermodynamic basis will be presented here for this difference in solubility. It is suggested by the following expression for the ratio of the solubility in α-Fe of carbon present in graphite and cementite, given by Darken (32):

$$\frac{[\text{wt\% C}]^{\text{gr}}_{\alpha\text{-Fe}}}{[\text{wt\% C}]^{\text{cem}}_{\alpha\text{-Fe}}} = \exp\left(\frac{-\Delta G^0_{\text{gr}\rightarrow\text{cem}}}{RT}\right). \qquad [1]$$

Depending upon the temperature, the solubilities can differ up to a factor of 200. It is clear that the thermodynamic properties of the contacting solids, graphite, and cementite, determine the difference in solubility. The same reasoning is applied here to gas mixtures with different composition in contact with iron or nickel, and which are considered to be in equilibrium respectively with graphite and cementite. This is illustrated here for a mixture of methane and hydrogen in contact with nickel:

$$CH_4(g) \rightleftarrows C(\text{in Ni}) + 2H_2(g)$$

The expression for the equilibrium constant for this reaction is derived from

$$\left(\frac{dG}{d\zeta}\right)_{P,T} = \mu_{C_{Ni}} + 2\mu^0_{H_2} - \mu^0_{CH_4} + RT\cdot\ln\frac{p^2_{H_2}}{p_{CH_4}} = 0. \qquad [2]$$

For the minor component of a binary solution, carbon in the present case, the chemical potential in the solution in nickel is given by (Blakely *et al.* (33) and Swalin (34))

$$\mu_{C_{Ni}} = \mu^0_{C,gr} + RT\cdot\ln\left(\gamma^0_{C,Ni}\cdot X_{C_{Ni}}\right) = \mu^0_{(C),C_{Ni}} + RT\cdot\ln(c_{C_{Ni}}) \qquad [3a]$$

in which for a diluted solution of carbon in nickel

$$\mu^0_{(C),C_{Ni}} = \mu^0_{C,gr} + RT\cdot\ln\left(\gamma^0_{C,Ni}\right) + RT\cdot\ln\left(\frac{M_{Ni}}{\rho_{Ni}}\right). \qquad [3b]$$

The expression for the equilibrium constant for a gas phase in equilibrium with a solution of carbon in nickel, finally becomes

$$K^{\text{sol}}_{CH_4/H_2} = \frac{p^2_{H_2}\cdot c^{\text{sol}}_{CH_4/H_2}}{p_{CH_4}} = \exp\left(\frac{-\left(\mu^0_{(C),C_{Ni}} + 2\mu^0_{H_2} - \mu^0_{CH_4}\right)}{RT}\right). \qquad [4]$$

The value of $K^{\text{sol}}_{CH_4H_2}$ is determined by the properties of the gas-phase components and Henry's law constant for the solution of carbon in nickel. It is clear that the solubility of carbon in nickel depends on the affinity for carbon formation of the gas phase: the higher the affinity for carbon formation (p_{CH_4} high or p_{H_2} low), the higher the solubility of carbon in nickel.

At the support side of the particle, the solubility is determined by the thermodynamic properties of the carbon filament, and differs from the graphite solubility. The solubility measurements of carbon in nickel in contact with a mixture of methane and hydrogen, performed by Yang *et al.* (35), confirm this. They observed that the carbon content at saturation was 35% higher than for a mixture in equilibrium with graphite.

Since the concentration of carbon, dissolved in nickel at the gas side of the nickel particle can exceed the solubility at the support side of the particle, a concentration gradient over the nickel particle becomes possible, and therefore, a driving force for the carbon diffusion through the nickel particle is created.

Thermodynamics of Carbon Filament Formation and Gasification

It was observed that the thermodynamic properties of filamentous carbon differ from those of graphite (6, 9–12). Rostrup-Nielsen (10) and Alstrup (12) attributed this to the structure of the carbon filaments, while Manning *et al.* (11) and De Bokx *et al.* (6) ascribed it to the formation of an intermediate carbide phase, which is not the final product, with different thermodynamic properties.

The purpose of this section is to describe the thermodynamics of the process of carbon filament formation. In this process, there is no direct contact between the gas phase and the final product, the filamentous carbon. The thermodynamics are usually derived from experiments by determining, for several temperatures, these conditions for which there is no carbon deposition nor gasification. This condition is usually referred to as the equilibrium for this reaction. It is preferable to refer to this condition as the "coking threshold," introduced by Wagner and Froment (36),

and to assign a "threshold constant" to it for the particular reaction since a number of steps are involved in the global mechanism for carbon filament formation that are different from the normal elementary surface reaction steps. Since it is nonreversible, the diffusion step has a behavior that is clearly different from that of a normal elementary surface reaction step. Under conditions away from the threshold, the diffusion of carbon through nickel takes place in one direction: from the gas side to the support side or the opposite. At the coking threshold, the rates of the surface reaction, the diffusion and the precipitation which operate in series, become zero.

At the support side of the particle, the equilibrium between filamentous carbon and carbon dissolved in nickel can be written

$$\mu_{C_{fil}} = \mu_{C_{Ni,r}} = \mu^0_{(C),C_{Ni}} + RT \cdot \ln c_{C_{Ni,r}}. \quad [5]$$

The equilibrium concentration of carbon dissolved in nickel at the support side of the nickel particle is the solubility of filamentous carbon in nickel (c^{sol}_{fil}), determined by the thermodynamic properties of filamentous carbon.

Since the rate of diffusion also becomes zero at the coking threshold, the concentration of carbon dissolved in nickel and its chemical potential are uniform over the whole particle and equal to the solubility of filamentous carbon in nickel:

$$c_{C_{Ni,f}} = c_{C_{Ni,r}} = c^{sol}_{fil}; \quad \mu_{C_{Ni,f}} = \mu_{C_{Ni,r}}. \quad [6]$$

At equilibrium, the chemical potential of carbon dissolved in nickel, just below the selvedge, and that of surface carbon are equal, so that

$$\mu_{C_a} = \mu_{C_{Ni,f}}. \quad [7]$$

Finally, the gas phase is in equilibrium with the surface carbon. In the case of methane cracking:

$$CH_4(g) \rightleftarrows C_a + 2H_2(g)$$

$$\left(\frac{\partial G}{\partial \zeta}\right)_{P,T} = \mu_{C_a} + 2\mu^0_{H_2} - \mu^0_{CH_4} + RT \cdot \ln\left(\frac{p^2_{H_2}}{p_{CH_4}}\right)_{eq} = 0. \quad [8]$$

Since at equilibrium, the chemical potential of carbon in all the consecutive steps has to be equal, the following relationships are valid:

$$\mu_{C_a} = \mu_{C_{Ni,f}} = \mu_{C_{Ni,r}} = \mu_{C_{fil}} = \mu^0_{CH_4} - 2\mu^0_{H_2} - RT \cdot \ln\left(\frac{p^2_{H_2}}{p_{CH_4}}\right)_{eq}. \quad [9]$$

It is clear that the final product, filamentous carbon, determines the gas-phase composition at the coking threshold, since it determines the chemical potentials of carbon dissolved in nickel and that of surface carbon. The threshold constant for methane cracking is then given by

$$K_M = \left(\frac{p^2_{H_2}}{p_{CH_4}}\right)_{eq} = \exp\left(-\frac{\Delta G^0_{C_{fil}}}{RT}\right) = \exp\left(-\frac{(\mu_{C_{fil}} + 2\mu^0_{H_2} - \mu^0_{CH_4})}{RT}\right). \quad [10]$$

The value of the threshold constant and the gas-phase composition at the coking threshold are determined by the thermodynamic properties of filamentous carbon. The threshold constant can be experimentally determined by measuring the partial pressures of methane and hydrogen for which the rate of carbon formation is zero.

A similar type of phenomenon, with the same type of driving force, was observed by Lamber *et al.* (37). They studied the interaction of highly dispersed nickel with amorphous carbon substrates between 700 and 1000 K and observed that carbon atoms dissolved in nickel and precipitated again as graphite: a conversion of amorphous carbon into graphitic carbon took place. This catalyzed conversion would proceed by a solution-precipitation mechanism, whereas the driving force is thought to be the difference in Gibbs free enthalpy between the initial and final forms of carbon. This causes probably different solubilities, so that a concentration gradient leading to carbon transport develops.

This is similar to the case of carbon filament formation from a gas phase: the global driving force for carbon filament formation is the difference in chemical potential between the gas phase and the carbon filament, and this causes different solubilities in Ni at the gas side and the support side of the particle and a concentration gradient leading to diffusion of carbon. The coking threshold can be interpreted as these conditions for which the gas phase carbon solubility equals the solubility of filamentous carbon.

Steady-State Growth and Gasification of Filamentous Carbon

For conditions leading to an affinity for carbon formation, there will be a net positive rate of carbon formation. Since at steady state the rates of the consecutive steps are equal, a certain concentration gradient develops, which is determined by the relative rates of the surface reaction and the carbon diffusion through the nickel particle:

$$r_C = r_{sr,net} = r_{C,diff} = \frac{D_{C,Ni}}{d_a} \cdot (c_{C_{Ni,f}} - c_{C_{Ni,r}}) \cdot a_{Ni}. \quad [11]$$

It is thereby assumed that the diffusion takes place through a slab with thickness equal to the average diffusion path length, d_a, and with a total area equal to the metal surface area, a_{Ni}. In Fig. 4, a number of possible situations are represented, depending upon the value of the diffusivity of carbon in nickel. A certain concentration gradient exists over the selvedge due to the segregation behavior. It is assumed that the diffusion through the selvedge is very fast,

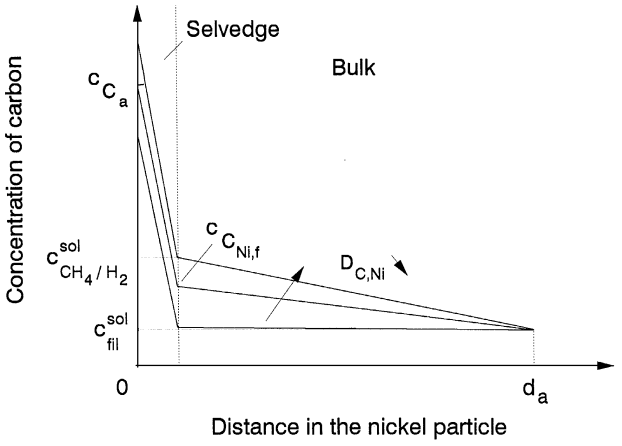

FIG. 4. Schematic representation of the concentration profile of carbon dissolved in the nickel crystallite during steady-state carbon filament growth, depending on the value of the carbon diffusivity in nickel $D_{C,\,Ni}$.

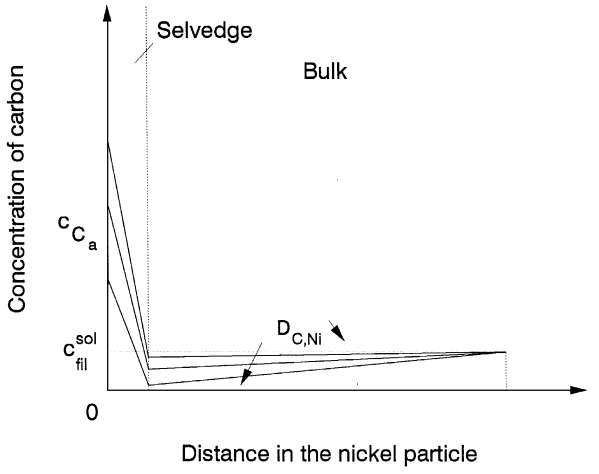

FIG. 5. Schematic representation of the concentration profile of carbon dissolved in the nickel crystallite during steady-state carbon gasification, depending on the value of the carbon diffusivity in nickel $D_{C,\,Ni}$.

so that there is an equilibrium between surface carbon and carbon dissolved in nickel just below the selvedge. For very high values of $D_{C,Ni}$, the concentration of carbon in nickel is almost uniform. For lower values of $D_{C,Ni}$, the concentration gradient cannot be neglected, so that the concentration of carbon at the gas side of the particle increases substantially. This is possible since the solubility of carbon in nickel is higher at the gas side of the particle. This will also cause the equilibrium surface coverage of carbon to increase, resulting in a higher rate of gasification of surface carbon and a lower net rate of carbon filament formation. Although the diffusion is clearly not the only rate-determining step, it influences the rate of carbon formation, due to its influence on the surface coverage of carbon. With a further decrease of the diffusivity, a maximum concentration gradient finally develops when the concentration at the gas side of the particle equals the gas-phase carbon solubility, so that the carbon diffusion can be said to be the only rate-determining step of the process.

When there is an affinity for gasification, the net rate of carbon formation is negative, and the concentration gradient is reversed (Fig. 5). The concentration at the support side of the particle is the solubility of filamentous carbon in nickel. Depending on the gasification conditions and the diffusivity, different profiles are obtained. The maximum concentration gradient is reached when the concentration of carbon dissolved in nickel at the gas side of the particle equals zero.

At the coking threshold, which separates the regions where there is an affinity for carbon formation and for gasification, the concentration of carbon dissolved in nickel is uniform and equal to the solubility of filamentous carbon.

Nucleation of Carbon Filaments

The situation which is encountered when a mixture with an affinity for carbon formation is contacted with a catalyst on which no filamentous carbon is present is represented in Fig. 6. A uniform concentration of carbon exists in nickel, equal to the gas-phase carbon solubility in nickel and higher than the saturation concentration of filamentous carbon. Nucleation of filamentous carbon can then take place, provided that the supersaturation is sufficiently high. Due to the very high concentration of carbon in nickel during nucleation and the segregation behavior, the surface coverage of carbon is very high, so that the net rate of the surface reactions is zero, although the mixture shows an affinity for carbon formation. After nucleation, the concentration at the support side of the particle drops to the saturation concentration of filamentous carbon, leading to one of the situations illustrated in Fig. 4.

Information concerning the nucleation of filamentous carbon, deposited by the methane cracking, was obtained

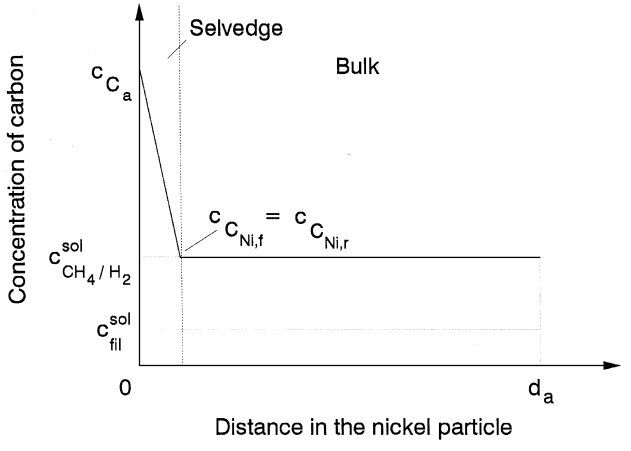

FIG. 6. Schematic representation of the concentration profile of carbon dissolved in the nickel crystallite during nucleation of filamentous carbon.

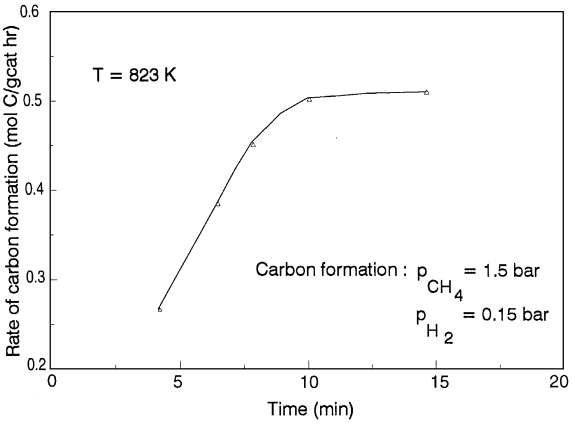

FIG. 7. Typical rate versus time curve for the methane cracking.

from an analysis of the weight versus time curves, and from experiments in which various carbon formation conditions were applied sequentially on the same catalyst sample. A typical weight versus time curve for the methane cracking, as shown in Fig. 7, has two zones: one with an increasing rate of carbon formation and one with a constant rate. The zone with decreasing rate, due to gradual deactivation of the catalyst, observed by Baker *et al.* (19) and Figueiredo (38), has not been observed in the methane cracking, except at $P_{CH_4} = 1.5$ bar and in the absence of hydrogen. A real induction period, during which the rate is zero, was only observed under conditions with a very low affinity for carbon formation. The period of increasing rate is ascribed to the nucleation time of the carbon filaments. It is likely that there is a large difference in the nucleation time of the filaments. Some filaments nucleate rapidly and probably reach a final growth rate, while other filaments are still nucleating. Once there is no further nucleation of new filaments, a constant rate of carbon formation is reached.

Valuable information can be obtained by sequentially applying two different carbon formation conditions on the same catalyst sample, followed by a gasification with hydrogen under the same conditions, as shown in Fig. 8. A condition with a low affinity for carbon formation (high p_{H_2}) was interrupted for a short time by a condition with a high affinity (low p_{H_2}). The rate of carbon formation under the conditions with a low affinity strongly increases after a short exposure of the sample to conditions with a high affinity for carbon formation. The subsequent rate of gasification (on a "used" catalyst) is much higher compared to the case where only the conditions with a low affinity are applied on a fresh catalyst sample and equals the rate of gasification that is observed if only the conditions with a high affinity are applied on a fresh catalyst sample. Furthermore, a new period of increasing rate of carbon formation is observed for the conditions with a high affinity for carbon formation, very similar to the period of increasing rate that is observed when an experiment is started on a fresh catalyst sample, although a constant rate of carbon formation was already reached under the conditions with a low affinity for carbon formation. Due to the scale of Fig. 8, this phenomenon cannot be clearly observed. Figure 9 clearly shows that this new period of increasing rate of carbon formation is longer and starts from a lower rate when the difference in affinity between the two conditions is larger.

These phenomena are explained by the higher number of growing filaments present under conditions with a high affinity for carbon formation. It is probable that for certain carbon filaments, a high supersaturation is required to nucleate, so that at conditions with a low affinity for carbon formation, only a small number of filaments nucleates. The higher number of filaments which nucleated during the conditions with a high affinity for carbon formation are able to grow further during the subsequent conditions with a low affinity, giving rise to an increased rate of carbon formation, or they can be gasified during the subsequent gasification, giving rise to an increased rate of gasification. This also explains the observation of the new period of increasing rate when conditions with a low affinity for carbon formation are followed by conditions with a high affinity.

This dependence of the number of growing filaments on the affinity for carbon formation must be taken into account when a kinetic modeling is performed of carbon filament formation. Not understanding this phenomenon can lead to a biasing of the experimental results and the kinetic modeling. It is comparable to performing rate measurements on catalysts with a different metal surface area, and combining the experimental results in the kinetic modeling.

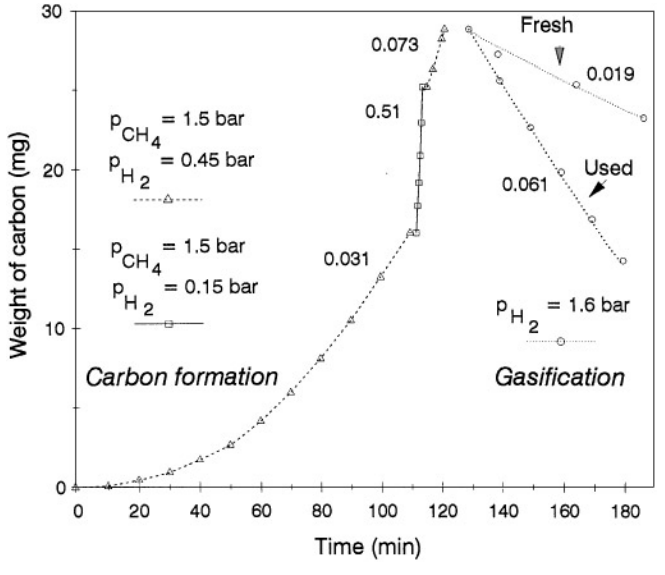

FIG. 8. Influence of the conditions with a high affinity for carbon formation on the subsequent conditions with a low affinity for carbon formation and on the rate of gasification. Carbon formation: $T = 823$ K; $p_{CH_4} = 1.5$ bar; $p_{H_2} = 0.15$ or 0.45 bar. Gasification: $T = 823$ K; $p_{H_2} = 1.6$ bar. Rates of carbon formation and of gasification (molC/gcat h) are indicated.

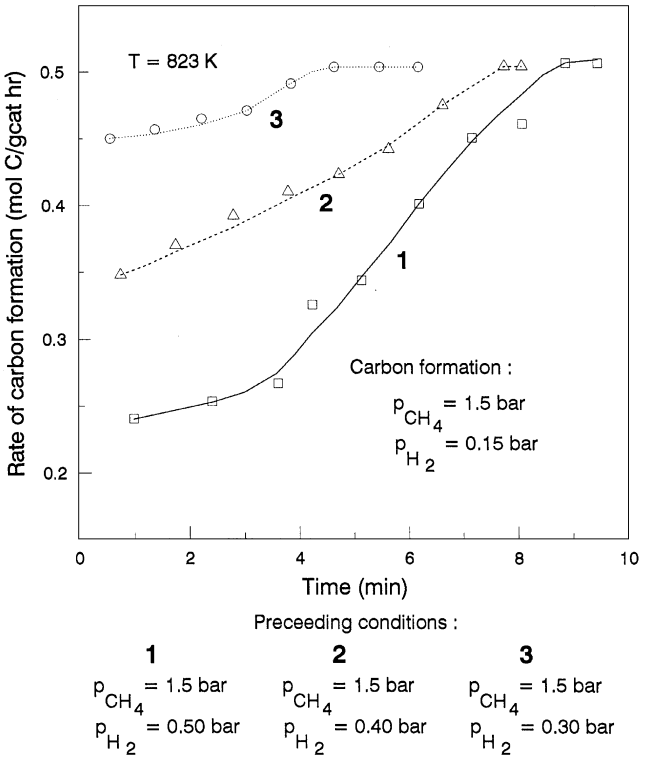

FIG. 9. Influence of the conditions with a low affinity for carbon formation on the "new" period of increasing rate of the subsequent conditions with a high affinity for carbon formation ($T = 823$ K; $p_{CH_4} = 1.5$ bar; $p_{H_2} = 0.15$ bar).

Initiation of Carbon Filament Growth and Formation of Hollow Carbon Filaments

The nucleation of filamentous carbon requires a supersaturation of carbon in nickel, followed by reconstruction and faceting of the particle and precipitation of graphitic layers (12, 18, 39). Deformation of the nickel particle takes place upon carbon filament formation. Whereas the faceting is considered as a necessary step for the filament formation (12, 18, 23), the deformation of the nickel particle with the formation of a pear shape is more probably a result of the carbon filament formation. In order to identify the driving force for the distortion of the nickel particle, the observation that the appearance of a pear-shaped, conical or dropwise particle accompanies the formation of hollow filaments is of importance (18, 25, 26, 40, 41).

It is proposed here that the deformation of the nickel particle and the appearance of hollow filaments is related to the relative rates of nucleation of carbon filaments and of diffusion of carbon through the nickel, and also to differences in diffusional path lengths on the metal/carbon interface that cause a difference in the rate of the carbon supply.

At low temperature, the rate of nucleation is low compared to the rate of diffusion. Nucleation is uniform over the whole metal/carbon (or support) interface, and the particle is nicely lifted from the support when carbon layers are excreted. Full filaments are formed, without hollow channel. A small deformation is possible, e.g., to a conical form, since as soon as nucleation has taken place, there will be a difference in excretion rates over the metal/carbon interface: those regions at the metal/carbon interface near the gas/metal interface, have higher excretion rates, since the diffusion path is shorter. When the particle is lifted more rapidly from the support near the gas/metal interface, a distortion is possible (Fig. 10), so that a conical particle can be obtained. The graphitic layers are conically ordered, as determined by the shape of the metal particles (Boellaard *et al.* (8) and Tracz *et al.* (25)). When there is no difference in diffusion path length, no deformation takes place, as observed by Murayama *et al.* (42). In the latter case, this observation may have been due to the fact that the metal particles were formed in situ in the gas phase, and were not localized on a support, so that no metal–support interaction had to be overcome.

At high temperature, nucleation is instantaneous, intrinsically much faster than the rate of diffusion. Nucleation occurs as soon as the supersaturation reaches the metal/support interface. The difference in diffusional path length causes rapid nucleation and excretion of carbon layers near the metal/gas interface, so that the metal is lifted from the support at these places. As soon as carbon excretion starts, the concentration of carbon in nickel drops sharply to the saturation concentration of filamentous carbon. Therefore, no driving force is present any longer for nucleation at places with high diffusional path lengths: no carbon excretion will take place there and hollow filaments are obtained (Fig. 11). At places where there is no excretion of carbon, the metal/support interaction must be overcome to lift the particle. As a result, a distortion takes place as the metal particle is lifted from the support near the gas/metal interface and sticks more strongly on the support far from it, so that a pear shape is obtained.

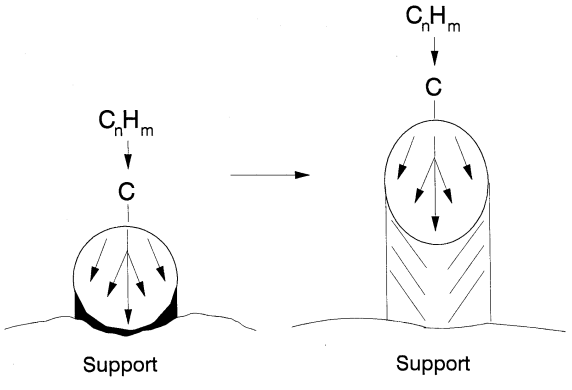

FIG. 10. Schematic representation of the deformation of the metal particle at low temperature/formation of full filaments.

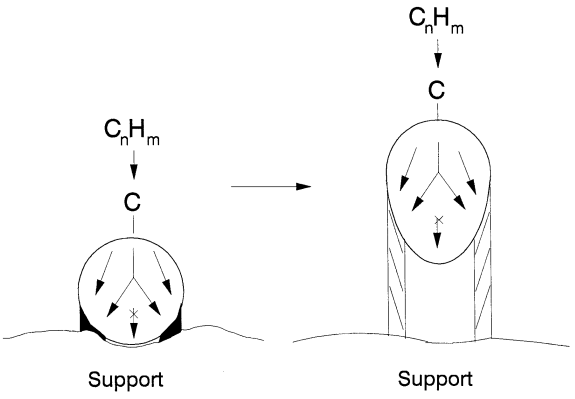

FIG. 11. Schematic representation of the deformation of the metal particle at high temperature/formation of hollow filaments.

Between these two mechanisms, an intermediate stage exists, which is a transition between full filaments and hollow filaments, as observed by Tracz *et al.* (25).

CONCLUSIONS

Based upon our own experimental results and literature information a detailed description is given of the formation and gasification of filamentous carbon. A rigorous thermodynamic description of the process of carbon filament formation is proposed. The gas-phase composition at the coking threshold is determined by the thermodynamic properties of filamentous carbon, the final product. Since filamentous carbon has a structure which differs from that of graphite, its thermodynamic properties are evidently different. The driving force for carbon diffusion and for the global process of carbon filament formation is the difference in solubility at the gas/metal interface and the carbon filament/metal interface. A thermodynamic basis for this difference in solubility is presented. At the coking threshold, the gas-phase carbon solubility equals the solubility of filamentous carbon in nickel.

According to the proposed model, the nucleation of filamentous carbon is caused by the formation of a solution of carbon in nickel that is supersaturated with respect to filamentous carbon. The degree of supersaturation is determined by the affinity for carbon formation of the gas phase. It was experimentally observed that the nucleation of filamentous carbon is much more difficult under conditions with a low affinity for carbon formation leading to a slow nucleation and very long periods of increasing rate of carbon formation, but also to a small number of carbon filaments that is finally able to nucleate under these conditions. This affects as well the rate of carbon formation as the rate of gasification observed in an electrobalance reactor unit.

It is proposed that the formation of hollow filaments and the deformation of the nickel particle are related to the relative rates of carbon diffusion through the nickel particle and carbon filament nucleation, and also to differences in diffusion path lengths on the metal/carbon interface.

APPENDIX: NOMENCLATURE

a_{Ni}	Nickel metal surface area (m^2/g_{cat})
$c_{C,a}$	Surface carbon concentration
$c_{C,Ni}$	Concentration of carbon dissolved in nickel ($molC/m^3_{Ni}$)
$c_{C,\{Ni,f\}}$	Concentration of carbon dissolved in nickel at the front of the particle, just below the selvedge (gas side) ($molC/m^3_{Ni}$)
$c_{C,\{Ni,r\}}$	Concentration of carbon dissolved in nickel at the rear of the particle (support side) ($molC/m^3_{Ni}$)
c^{sol}_{fil}	Solubility of filamentous carbon in nickel ($molC/m^3_{Ni}$)
$c^{sol}_{CH_4H_2}$	Solubility of carbon in nickel in contact with a gas phase consisting of methane and hydrogen ($molC/m^3_{Ni}$)
d_a	Average diffusion path length (m)
$D_{C,Ni}$	Diffusivity of carbon in nickel (m^2/h)
M_{Ni}	Molecular weight of Ni (g/mol)
$K^{sol}_{CH_4H_2}$	Equilibrium constant for the equilibrium between a gas phase containing methane and hydrogen and carbon dissolved in nickel
K_M	Threshold constant for the methane cracking
p_i	Partial pressure of component i
r_C	Rate of carbon filament formation (molC/gcat h)
$r_{sr,net}$	Net rate of the surface reactions (molC/gcat h)
$r_{C,diff}$	Rate of carbon diffusion through nickel (molC/gcat h)
$[wt\%\ C]^{gr}_{\alpha\text{-Fe}}$	Solubility in α-Fe of carbon present in graphite
$[wt\%\ C]^{cem}_{\alpha\text{-Fe}}$	Solubility in α-Fe of carbon present in cementite
$X_{C,Ni}$	Bulk molar fraction of carbon dissolved in nickel
$\gamma^0_{C,Ni}$	Henry's law constant for carbon in solution in nickel
$\Delta G^0_{C,fil}$	Standard Gibbs free enthalpy change for the formation of filamentous carbon
$\Delta G^0_{gr\rightarrow cem}$	Standard Gibbs free enthalpy change for the formation of cementite from graphite
$\mu_{C\{Ni\}}$	Chemical potential of carbon dissolved in nickel
$\mu^0_{C,gr}$	Standard chemical potential of graphite
$\mu^0_{(c),\{C,Ni\}}$	Standard chemical potential chosen if the amount of carbon dissolved in nickel is expressed as a concentration

$\mu_{C,fil}$ Chemical potential of filamentous carbon
$\mu_{C,a}$ Chemical potential of adsorbed carbon
$\mu_{C,\{Ni,f\}}$ Chemical potential of carbon dissolved in nickel at the front of the particle, just below the selvedge (gas side)
$\mu_{C,\{Ni,r\}}$ Chemical potential of carbon dissolved in nickel at the rear of the particle (support side)
ρ_{Ni} Density of Ni (g/m^3)
ζ Extent of reaction

ACKNOWLEDGMENT

This study was financially supported by ICI KATALCO, Billingham, UK.

REFERENCES

1. Trimm, D. L., *Catal. Rev.-Sci. Eng.* **16**, 155 (1977).
2. Bartholomew, C. H., *Catal. Rev.-Sci. Eng.* **24**, 67 (1982).
3. Rostrup-Nielsen, J. R., Catalytic steam reforming, *in* "Catalysis, Science and Technology," Vol. 5, p. 1. Springer, Berlin, 1984.
4. McCarty, J. G., and Wise, H., *J. Catal.* **57**, 406 (1979).
5. McCarty, J. G., Hou, P. Y., Sheridan, D., and Wise, H., *in* "Coke Formation on Metal Surfaces" (L. F. Albright and R. T. K. Baker, Eds.), ACS Symposium Series 202, p. 253. Am. Chem. Soc., Washington, DC, 1982.
6. De Bokx, P. K., Kock, A. J. H. M., Boellaard, E., Klop, W., and Geus, J. W., *J. Catal.* **96**, 454 (1985).
7. Kock, A. J. H. M., De Bokx, P. K., Boellaard, E., Klop, W., and Geus, J. W., *J. Catal.* **96**, 468 (1985).
8. Boellaard, E., De Bokx, P. K., Kock, A. J. H. M., and Geus, J. W., *J. Catal.* **96**, 481 (1985).
9. Dent, F. J., Moignard, L. A., Eastwood, A. H., Blackburn, W. H., and Hebden, D., *Trans. Inst. Gas. Eng.* 602 (1945–1946).
10. Rostrup-Nielsen, J. R., *J. Catal.* **27**, 343 (1972).
11. Manning, M. P., Garmirian, J. E., and Reid, R. C., *Ind. Eng. Chem. Process Des. Dev.* **21**, 404 (1982).
12. Alstrup, I., *J. Catal.* **109**, 241 (1988).
13. Rostrup-Nielsen, J. R., and Trimm, D. L., *J. Catal.* **48**, 155 (1977).
14. Buyanov, R. A., Chesnokov, V. V., and Afanas'ev, A. D., *Kinet. Katal.* **20**, 166 (1979).
15. Buyanov, R. A., *Kinet. Katal.* **21**, 189 (1980).
16. Sacco, A., Jr., Thacker, P., Chang, T. N., and Chiang, A. T. S., *J. Catal.* **85**, 224 (1984).
17. Sacco, A., Jr., Geurts, W. A. H., Jablonski, G. A., Lee, S., and Gately, R. A., *J. Catal.* **119**, 322 (1989).
18. Yang, R. T., and Chen, J. P., *J. Catal.* **115**, 52 (1989).
19. Baker, R. T. K., Barber, M. A., Harris, P. S., Feates, F. S., and Waite, R. J., *J. Catal.* **26**, 51 (1972).
20. Baker, R. T. K., Alonzo, J. R., Dumesic, J. A., and Yates, D. J. C., *J. Catal.* **77**, 74 (1982).
21. Baker, R. T. K., and Chludzinski, J. J., *J. Phys. Chem.* **90**, 4734 (1986).
22. Kim, M. S., Rodriguez, N. M., and Baker, R. T. K., *J. Catal.* **131**, 60 (1991).
23. Kim, M. S., Rodriguez, N. M., and Baker, R. T. K., *J. Catal.* **134**, 253 (1992).
24. Lobo, L. S., and Trimm, D. L., *J. Catal.* **29**, 15 (1973).
25. Tracz, E., Scholz, R., and Borowiecki, T., *Appl. Catal.* **66**, 133 (1990).
26. Tibbetts, G. G., *J. Cryst. Growth* **66**, 632 (1984).
27. Schouten, F. C., Kaleveld, E. W., and Bootsma, G. A., *Surf. Sci.* **63**, 460 (1977).
28. Laguës, M., and Domange, J. L., *Surf. Sci.* **47**, 77 (1975).
29. Isett, L. C., and Blakely, J. M., *Surf. Sci.* **47**, 645 (1975).
30. Isett, L. C., and Blakely, J. M., *Surf. Sci.* **58**, 397 (1976).
31. Vajo, J. J., and McCarty, J. G., *Appl. Surf. Sci.* **47**, 23 (1991).
32. Darken, L. S., and Gurry, R. W., "Physical Chemistry of Metals." McGraw-Hill, New York, 1953.
33. Blakely, J. M., and Shelton, J. C., Equilibrium adsorption and segregation, *in* "Surface Physics of Materials" (J. M. Blakely, Eds.), Vol. I. Academic Press, New York, 1975.
34. Swalin, R. A., "Thermodynamics of Solids." Wiley, New York, 1962.
35. Yang, R. T., Goethel, P. J., Schwartz, J. M., and Lund, C. R. F., *J. Catal.* **122**, 206 (1990).
36. Wagner, and Froment, G. F., "Hydrocarbon Processing," p. 69. July 1992.
37. Lamber, R., Jaeger, N., and Schulz-Ekloff, G., *Surf. Sci.* **197**, 402 (1988).
38. Figueiredo, J. L., and Trimm, D. L., *J. Appl. Chem. Biotechnol.* **28**, 611 (1978).
39. Eizenberg, M., and Blakely, J. M., *Surf. Sci.* **82**, 228 (1979).
40. Zaikovskii, V. I., Chesnokov, V. V., and Buyanov, R. A., *Appl. Catal.* **38**, 41 (1988).
41. Baker, R. T. K., *in* "Catalyst Deactivation 1991" (C. H. Bartholomew and J. B. Butt, Eds.), p. 1. 1991.
42. Murayama, H., and Maeda, T., *Nature* **345**, 791 (1990).